



CHORUS

This is the accepted manuscript made available via CHORUS. The article has been published as:

Molecular dynamics characterization of the contact between clean metallic surfaces with nanoscale asperities

Hojin Kim and Alejandro Strachan

Phys. Rev. B **83**, 024108 — Published 31 January 2011

DOI: [10.1103/PhysRevB.83.024108](https://doi.org/10.1103/PhysRevB.83.024108)

**Molecular dynamics characterization of the contact
between clean metallic surfaces with nanoscale asperities**

Hojin Kim and Alejandro Strachan

School of Materials Engineering and Birck Nanotechnology Center

Purdue University, West Lafayette, Indiana 47907, USA

We use molecular dynamics (MD) simulations to characterize the tensile strength of contacts formed between various clean platinum surfaces with nanoscale asperities. Both commensurate contacts between (001) and (111) surfaces and incommensurate (001) ones are considered over wide range of asperity sizes. In cyclic closing and opening, fresh asperities that form contacts for the first time shows significant plastic deformation; this leads to a reduction in the effective contact area during the first few cycles after which steady state is achieved both in terms of contact size and the pull-out force necessary to open the contacts. As is the case for commensurate surfaces [Kim and Strachan, Phys. Rev. Lett. **104**, 215504 (2010)] the strength of the metallic bridges that form in incommensurate contacts exhibit strong size effects; their strength increases with decreasing size until a length of approximately 5 nm below which weakening is observed. Commensurate contacts lead to stronger bridges than incommensurate ones but only during the initial closing events, after steady state is achieved commensurate and incommensurate (001) surfaces lead to bridges of similar strengths.

I. Introduction

A fundamental understanding of the mechanical behavior of contacting surfaces with nanoscale asperities including their adhesion and friction is critical for a wide range of applications including nano- and micro-scale switches for radio frequency^{1,2} and low-power electronics³ applications. From a basic science point of view nanoscale contact experiments^{4,5} and simulations⁶⁻⁸ between clean surfaces can shed light into the mechanical properties of nanosize materials with sub-100 nm size scales; an important and interesting regime not accessible by other experimental means and that remains essentially unexplored. In this paper we use molecular dynamics (MD) to investigate the strength of the metallic bridges that form when two clean platinum surfaces with nanoscale asperities are brought together focusing on the effect of contact size and repeated contact closing and opening.

The development and improvement of experimental tools such as scanning tunneling microscope (STM)⁹ and the mechanically controllable break junction (MCBJ)¹⁰ have contributed significantly to our understanding of nanosize metallic contacts and atomic-level simulations are providing important insight regarding the atomic level processes that govern contact physics.⁶⁻⁸ Our recent molecular dynamics (MD) simulations show that the strength of nanoscale contacts between commensurate surfaces is size-dependent and exhibit a maximum for contact lengths of approximately 5 nm. Despite such advances several questions regarding the behavior of contact with sub-100 nm linear dimensions remain. We focus on how cyclic contact opening and closing affect asperity shape and

subsurface defects and extend our previous work on size-dependent contact strength⁶ to incommensurate surfaces.

Real metallic surfaces in microdevices exhibit nanoscale roughness with asperities with various shapes and sizes and exhibit complex surface chemistry that depends on fabrication operating environment. When two rough surfaces are brought together, various nanosized contact spots will form with a distribution of sizes and local stresses. The first asperity peaks to make contact will experience a large compressive stress and will often deform plastically until the effective contact area is large enough to withstand the closing force; thus the hardness of a material is very important in contact physics. The resulting effective contact area and the nature of the contacts play an important role in determining the pull-out force needed to open the contact a critical parameter in the design on nano- and micro-switches. Adhesion between the contacting surfaces also depends on their chemistry and environment (e.g. humidity), surface roughness. Under normal operating conditions noble metal surfaces exhibit a layer of adsorbed molecules that play a large role in contact mechanics. These surface films provide damping for the impact during closing and also affect adhesion by influencing capillary forces and limiting direct metal-metal interactions¹¹. Despite these pervasive molecular films, in most cases we expect some direct metal-metal bridging due to the large local stresses, plastic deformation within the asperities, as well as to the large local temperatures caused by Joule heating when electrical currents run through the contacts. Local melting, mass transfer, and metallic bridging have been observed in microswitches.^{12, 13} Thus,

understanding the mechanical response of the nanoscale metallic bridges that form between the surfaces is of great interest.

This paper is organized as follows: in Section II we provide simulation details, in Section III we describe the evolution of surface properties with cyclic loading and Section IV focuses on the size dependent strength of the nanoscale contacts. A discussion of the meaning and relevance of our results is presented in Section V and conclusions are drawn in Section VI.

II. Simulation details

All simulations are carried out with the simulation package LAMMPS¹⁴ from Sandia National Laboratories. We employ a many body embedded atom method (EAM) potential to define the interaction between Pt atoms¹⁵. This potential was parameterized to reproduce the equilibrium lattice constant, sublimation energy, elastic constants, and vacancy formation energy of Pt from experimental data.

A. Initial structures and contact closing and opening procedure

We simulate the contact two clean platinum (Pt) slabs with (111) and (001) surfaces with nanoscale asperities. Figure 1 shows a snapshot of one of our initial models and geometrical details of all simulations are given in the Table 1. We use a sinusoidal profile as an initial surface roughness; the top and bottom surfaces are obtained using the following surface profile:

$$Z_{initial} = MIN \left[A \sin \left(\frac{2\pi x}{\lambda_x} \right), A \sin \left(\frac{2\pi y}{\lambda_y} \right) \right] \quad (1)$$

as in our previous study ⁶ the asperity height parameter A is 1 nm and the peak to peak (λ) distance is half of the simulation cell. This leads to four asperities in each simulation cell and asperity peaks in the top and bottom surfaces are perfectly aligned with each other. We use samples with (111) surfaces with commensurate contacts [these configurations will be denoted c-(111)] and (001) both with commensurate [c-(001)] and incommensurate [i-(001)] contacts. The incommensurate contact is obtained by rotating one of the slabs by 45° around the [001] direction; a small strain (between 0.4 and 0.03%) is applied so that both slabs have identical cross-sections. To perform cyclic closing and opening of the contact we use the following procedure:

i) The two slabs are placed with 1 nm separation and the system is thermalized for 30 ps using isothermal MD (NVT ensemble).

ii) Contacts are closed via constant-energy MD simulations (NVE ensemble) for 180 ps where external forces are applied to both slabs in opposite directions. The force is applied to atoms within a thin slice (4.5 nm thick) next to the free surfaces away from the contacting ones. The external force is chosen to result in an overall compressive stress (ratio between total force and the cross sectional area of the simulation cell) of -100 MPa.

iii) The applied force is reversed to open the contact in a stepwise fashion with steps of 100 MPa (with resulting stress of 0, 100MPa, 200MPa, ...) and at each stress level an NVE simulation is performed for 10 ps. This is continued until the contact opens.

Multiple contact simulations are performed by repeating the entire procedure starting from step i) with the structure resulting at the end of step iii). Depending on system size we performed between 1 and 25 closing and opening cycles. From these simulations we obtain the pull-out force, the force required to open the contact. Contact opening is determined by monitoring the temporal evolution of the kinetic energy, a steep increase in kinetic energy denotes opening. The strength of the nanoscale contacts is defined as the ratio between the pull-out force and the effective contact area (computed as described below).

B. Simulation analysis

To determine the tensile strengths of the metallic bridges formed during contact we compute the actual contact area (A_{contact}) when the contact is closed. A_{contact} is obtained from the atomic positions using a 2-dimensional grid with spacing 0.5 Å. We project the positions of atoms within 2.0 Å of the thinnest contact region on the x-y plane and mark all grid points within a radius of 1.97 Å of the atomic center. All empty grid points completely surrounded by the originally marked points are subsequently checked. We obtain the actual contact area from the number of occupied grid spaces (N_{grid}) as $A_{\text{contact}} = N_{\text{grid}} \times A_{\text{grid}}$ where A_{grid} is $0.5 \times 0.5 \text{ \AA}^2$. The contact length (l_c) is then computed as the square root of average contact area per asperity ($A_{\text{contact}}/4$ in our case).

In order to study the role of sub-surface defects on the mechanical response of the contact, we classify individual atoms as perfect fcc atoms, surface atoms and atoms with hexagonal close packed (hcp) bonding environments using a

combination of i) coordination number (Z) obtained using a cutoff distance of 3.3 Å and ii) the centrosymmetry parameter (P)¹⁶, defined as $P = \sum_{i=1,6} |r_i + r_{i+6}|^2$ where r_i and r_{i+6} are the vectors corresponding to the six pairs of opposite nearest neighbors in the fcc lattice. This last parameter is useful to distinguish atoms in fcc environments (that are centrosymmetric) from hcp ones. Based on these two scalars, obtained for every atom in the systems, we classify atoms as: i) fcc (Z=12 and P<5), ii) hcp (Z=12 and 5<P<14), and iii) other defects which are mostly surface atoms. Dislocations in fcc crystals dissociate into two partial dislocations that are separated by a stacking fault ribbon. Stacking faults are formed by two consecutive planes of hcp atoms. Since individual dislocation lines are not easily identifiable in finite temperature, large-scale MD simulations, we consider the number of hcp atoms as a measure of dislocation activity. In cases where only leading partial dislocations dominate plasticity (this has been observed in nanoscale materials lacking enough space for the nucleation of partial dislocations following the leading partials, see Ref. [17] and references therein) the number of hcp atoms are proportional to the area swept by the partials and consequently plastic strain. In cases involving both leading and trailing partials the number of hcp atoms are approximately proportional to the total dislocation line length since the width of the stacking fault ribbon is rather constant throughout the dislocations. In both cases, as well as for intermediate conditions, the number of hcp atoms provides a measure of dislocation-based plasticity.

III. Evolution of area, opening force and plasticity during cyclic contacts

Figure 2 shows the effective contact area per asperity obtained from our simulations as a function of the radius of curvature of the initial asperities evaluated at the asperity peaks given by,

$$R = \left[\frac{(1 + f'(x)^2)^{3/2}}{|f''(x)|} \right]_{x=apex}, f(x) = A \sin\left(\frac{2\pi}{\lambda}x\right) \quad (2)$$

where prime denotes derivative with respect to x . Open symbols in Fig. 2 denote the 1st contact and closed symbols are the averaged value of multiple contacts (we note that in the later case asperity curvatures would have evolved as we will discuss below). Thus, our large-scale simulations enable us to explore the mechanical response of contacting bridges with cross-sectional areas between just over 1 nm² and 100 nm². As mentioned earlier, this size-scale regime is very important for applications involving nano- and micro-switches but not well understood.

Cyclic contact operation is expected to alter the shape of the asperities, resulting in changing the effective contact area and surface adhesion. We find a decrease in effective contact area during cyclic contact as asperities become steeper due to plastic deformation during pullout. Figure 3 shows the evolution of the effective contact area (circles) and pullout force (triangles, displayed on the right y-axes) for the three surfaces types with similar simulation cell sizes (corresponding to peak-to-peak distance of ~12.5 nm). We observe a significant decrease in effective contact area from the 1st contact between fresh, defect-free asperities and the second between nano-asperities that have undergone plastic

deformation. As the effective contact area decreases with cyclic contact operation so does the pull-out force and after a few contact cycles, steady state is reached both in the evolution of contact area and pull-out force. We see from Fig. 3 that the two commensurate contacts of (111) and (001) surfaces exhibit a larger degree of area reduction than the incommensurate ones; this is observed for all sizes we studied.

To investigate the atomic level processes that govern the evolution of the effective contact area and pull-out force that control plastic deformation, we study the temporal evolution of the number of hcp atoms (that, as describe earlier, provide information regarding dislocation activity) during cyclic loading. Figures 4(a-c) show the number of hcp atoms (normalized by the effective contact area when the contact is closed) as a function of time for the 1st (circles) and last contacts (triangles) for the same cases as in Fig. 3. During first contact closing (up to a time slightly longer than 200 ps marked with vertical lines) we observe an increase in the number of hcp atoms as the asperities experience a large compressive stress and deform plastically. In all cases the number of hcp atoms increases approximately to the same value (50 per nm² of effective contact area). Interestingly, during contact closing for commensurate and incommensurate (001) surfaces the number of hcp atoms reaches maxima and then decrease; these maxima are associated with an overshoot caused by the initial impact during contact closing. The velocity at impact is known to be an important design parameter to improve the performance and reliability of micro-switches.¹⁸ As the compressive load is transformed into tensile load during opening the number of

hcp atoms in the two (001) surfaces decreases as some of the partial dislocations trace back their steps. This does not happen in the (111) case since trailing partial nucleation is observed following the leading partials; the resulting full dislocations form complex structures that can not trace back their steps as easily as the single leading partials in (001) cases.

We now turn to the process of contact opening. In all cases opening leads to large bursts of dislocation activity; this is necessary to produce the plastic deformation necessary prior to separation of the metallic contacts. For all surfaces, the first opening involves more plastic deformation than subsequent ones and this is consistent with the large reduction in contact area between the first and second cycles seen in Fig. 3. Interestingly, plastic deformation activity as measured by the number of hcp atoms produced correlates with the degree of reduction in the contact area. (111) surfaces generate the largest amount of hcp atoms and also shows the largest decrease in effective contact area; on the other hand, the incommensurate (001) contacts exhibits the smallest amount of plastic deformation and reduction in contact area. While Figure 4 shows only the first and last contact cycles, we find that after a few contact events, as the contact area and pull-out force reach steady state the underlying atomic processes do so as well.

IV Size-dependent strength of nanoscale contacts

A. Strength vs. size

Figure 5 shows the local stress on the metallic bridges required to open them as a function of contact length (defined as the square root of the effective contact area per asperity) for all surfaces. The results in Ref. [6] for commensurate contacts are reproduced here for comparison. As was reported earlier for commensurate contacts we find the tensile strength of nanoscale contacts between incommensurate surfaces to be strongly size dependent. These size effects are observed both for the 1st opening after fresh asperities are brought together, Fig. 5(a), and for multiple contacts, Fig. 5(b). The results in Figure 5(b) are averaged over multiple contacts after steady state is achieved. For all surfaces, the tensile strength of the bridges increases as their size is decreased until they reach a length of approximately 5 nm. This is consistent with the general observation of “smaller is stronger” seen in a variety of metallic systems including polycrystals and micro-pillars. However, nanoscale contacts show a maximum in tensile strength for a finite size and further reduction in bridge length leads to weakening. As shown in Ref. [6] both for initial and steady state contacts (111) surfaces form stronger bridges than (001) surfaces. This is expected since the slip planes in the (001) contacts make an angle of 54.7° with the tensile axis resulting in a larger Schmidt factor (ratio between the shear stress resolved in a slip system and that applied tensile load) than for (111) surfaces where the corresponding angle is 70.5° . For fresh asperities we also find that the commensurate (001) bridges are stronger than their incommensurate counterparts. Note that the difference in strength is approximately 20%, this should be contrasted with friction studies involving shear stress on the contact

plane where incommensurate surfaces often exhibit friction coefficients significantly lower than those in commensurate cases^{19,20}. Interestingly, the initial difference in strength between commensurate and incommensurate contacts all but disappears for multiple contacts.

B. Atomic processes of nano-contact plasticity

Strengthening with decreasing characteristic size has been observed for a variety of crystalline metals, from polycrystalline metals¹⁷ to single crystal micro-pillars.^{21,22} The underlying mechanisms believed to govern strengthening with decreasing size can be grouped in two categories: i) a decrease in the initial density of mobile dislocations available for plastic deformation, or ii) an inability of the material to increase the density of mobile dislocations during deformation.^{21,22} Thus, in order to characterize the underlying physics behind the observed size dependence of contact strength we study how the initial dislocation density and the production of new dislocations during deformation depend on contact size. In both cases we normalize the number of hcp atoms by the effective contact area in the closed configuration. Figure 6 shows the initial number of hcp atoms prior to opening [Figs. 6(b) and (d)] and the production of hcp atoms during contact opening [Figs. 6 (a) and (c)] as a function of contact size for the initial (top row) and steady state (bottom row) cases. The number of hcp atoms available before opening is defined as the minimum between closing and opening and is taken as a measure of dislocations available for plastic deformation during opening. The production of hcp atoms during opening is defined as the difference between the

maximum number of hcp atoms during opening and the previous minimum, see Fig. 4; this is taken as a measure of the increase in dislocation density during plastic deformation either by growing existing dislocations or nucleating new ones. The initial number of hcp atoms originates from the dislocations and other defects produced during closing (for the initial contacts) or cyclic contact operation (for steady state conditions).

Figures 7, 8 and 9 complement Fig. 6 and help understand the atomic origin of size effects. We show atomistic snapshots for the three surfaces corresponding to closed contact (top rows), before contact opening [configuration with lowest number of hcp atoms (middle rows)] and during opening (bottom). For each surface we show three contact sizes with the center column corresponding to the strongest size. Large dark spheres in Figs. 7-9 correspond to hcp atoms and smaller ones show fcc atoms. The production of hcp atoms during opening per unit contact area increases approximately linearly with contact size (L) for all cases studied, see Figs. 6(a) and (c) (solid lines represent linear functions). This indicates that the plastic zone extends a distance proportional to L into the contacts forming a 3D region of plastic deformation. This scaling does not indicate an inability to increase the number of dislocations with decreasing size and, thus, we discard this as a possible mechanism of size effects in contact strength not just for commensurate contacts as in Ref. [6] but for incommensurate as well. For initial contacts between commensurate (001) surfaces, the number of defects prior to opening decreases with decreasing contact size and becomes essentially zero for a finite contact size that

corresponds to the strongest contact. This can be confirmed from the snapshots in Fig. 7; we see no dislocations in the contacts before to opening for sizes equal or less to the one corresponding to the strongest size. c-(111) and i-(001) contacts lead to larger concentration of defects prior to opening and the number does not go to zero for the strongest contact size. However, inspection of the atomic snapshots in Figs. 8 and 9, reveals that the density of defects available prior to opening (middle row of snapshots) has reduced significantly when the strongest contact size is reached (middle column of Figs. 8 and 9). More importantly, the hcp atoms remaining do not form dislocations that can contribute to plastic deformation during contact opening. In the case of (111) surfaces we observe planes of hcp atoms located at the contacts oriented perpendicular to the loading axis; they represent twins and stacking faults. There is no resolved shear stress on the plane of these defects and consequently they do not facilitate plastic deformation during opening. The incommensurability of i-(001) cases makes it impossible to have defect-free contacts as in the case of c-(001). However, we find that for the strongest size in i-(001) surfaces no dislocations are present before contact opening while dislocations can clearly be seen for larger cases (right column of Fig. 9). Snapshots for the i-(001) with cross-section $40 \times 40 \text{ nm}^2$ is shown in the supplementary material.²³ In summary, the maximum in contact strength corresponds to the size where the initial number of mobile dislocations available prior to contact opening is zero.

Weakening for contact sizes below 5 nm has been attributed to the possibility of simple slip inside the contact region for commensurate contacts. Figure 8

confirms the same physics for i-(001) case. We see that plastic deformation for the smallest contacts is restricted to the contact neck region while the plastic zone in contacts with higher aspect ratios necessarily extends into the bulk of each slab. Larger pull-out forces are necessary to move dislocations that glide into the bulk of the contacts due to the lower local stresses as compared to the neck region and dislocation pileups; this causes strengthening.

IV. Discussion

A. Contact evolution with cyclic closing and opening

In all cases we studied, plastic deformation during the first few contact openings leads to steeper asperities and a reduction of effective contact area; after a short transient of a few contact closing/opening cycles the effective contact area, asperity shape, and pull-out force achieve steady-state values and so do the sub-surface defects. This may seem to contradict the experimental observation of an increase in adhesion force and effective contact area during the first cycles of operation of micro-switches.²⁴ The likely reason for the later observation is plastic deformation as scales larger than that of individual asperities that causes a large number of asperities to come into contact. Also, surface passivation present in real devices will influence asperity size evolution; these cases are beyond the scope of this paper where we focus on clean surfaces.

B. Atomic processes that govern size effects

A detailed analysis of the MD trajectories enables us to understand the atomic origin of such interesting size dependent mechanical response. We find a reduction in the density of dislocations available when the contact is opened as contact size is reduced down to the strongest contact size (~5 nm) where we observe essentially no mobile dislocations. Thus, we attribute a decrease in initial dislocation density as responsible for the contact strengthening with decreasing size as opposed to an inability to increase dislocation density (see, Fig. 6) as seems to be the case for micropillars.²¹ Further reduction in contact length leads to weaker contacts due to a reduction in constraints to plastic deformation caused by the bulk of each contacting slab. Contacts with low aspect ratios (small lengths) enable for plasticity to occur via simple dislocation glide inside the contact bridge, with the dislocation nucleating on one side of the bridge and emerging out from the opposite one. In contrast, in wires with larger contact areas dislocations necessarily need to glide into the slabs where pileups and a lower stress leads to higher stresses being necessary for their motion, see Figs. 7, 8 and 9. This explains the weakening below 5 nm and why the strongest contact is slightly smaller in (111) surfaces (with slip planes making steeper angles with the tensile axis) than (001) ones, see Fig. 5. Recently, a new mechanism to nucleate partial dislocations and produce intrinsic stacking faults, denoted near surface nanodisturbances, has been proposed to operate on nanowires at low temperatures.²⁵ While our analysis and visual inspection have not indicated the presence of nanodisturbances the focus of this paper is not on the nucleation of the defects responsible for plastic deformation; additional simulations and

analysis would be required to provide a definite answer regarding defect nucleation in nanoscale contacts (both in between virgin surfaces and after cyclic contact operation).

C. Role of surface orientation

The strength of the initial contact between fresh, incommensurate (001) surfaces is smaller than that of their commensurate counterparts; interestingly, after a few contact closing and opening cycles contacts between these two surfaces plastic deformation at the asperities leads to essentially identical strengths. Incommensurate contact formed the weakest bridges at comparable contact sizes while commensurate of (111) surface result in the strongest contacts.

V. Conclusions

We characterized the mechanical strength of the nanoscale metallic bridges that form when contacts between two clean Pt surfaces with nanoscale asperities are repeatedly brought into contact and separated. We simulated commensurate (111) surfaces and commensurate and incommensurate (001) surfaces. Starting with surfaces with sinusoidal asperity shapes we find that plastic deformation during contact closing and opening leads to asperities becoming steeper and a reduction in effective contact area during the first few cycles after which steady state is achieved in terms of asperity shape and pull out force.

We find that incommensurate (001) contacts exhibit a strong size dependency with the same trends reported for commensurate contacts in Ref. [6]. In all cases studied, we find a strongest contact size of approximately 5 nm. While a maximum in strength has been observed in nanocrystals as grain size is reduced, nanoscale contacts represent the first time this effect is seen in single crystalline materials. This work shows that nanoscale contact experiments could provide invaluable information regarding the mechanical response of materials with sub-100 nm regime.

Acknowledgements

This work was supported by the US Department of Energy's National Nuclear Security Administration under contract Grant No. DE-FC52-08NA28617. Computational resources from nanoHUB.org are gratefully acknowledged.

Table 1. Details of MD simulation cells

<i>Orientation</i>	<i>Slab size (nm)</i>	<i>Total</i>	<i>N_{cycle}</i>
(001)	9.8×9.8×20	233208	23
	14.9×14.9×20	538960	13
	24.7×24.7×20	1481640	8
	39.2×39.2×20	3731496	7
	49×49×20	5833496	2
	98.1×98.1×20	23333984	1
(111)	10.1×9.99×20	252244	25
	14.9×14.98×20	558584	16
	24.99×24.97×20	1562360	9
	49.84×49.95×20	6249112	5
	99.97×99.89×20	24997808	1
Incommensurate	10.6×10.6×20	27782	25
	14.98×14.98×20	557620	18
	25.5×25.5×20	1625854	9
	38.8×38.8×20	3765874	6
	48.2×48.2×20	5814056	4
	96.5×96.5×20	23256660	1

Figure captions

Figure 1. Snapshot of metal-metal contact.

Figure 2. Effective contact areas obtained by grid-based analysis corresponding to the radius of asperity curvatures at all surfaces

Figure 3. Evolution of effective contact area and pull-out force as a function of contact cycle for (a) commensurate (001), (b) incommensurate of (001), and (c) (111) surfaces with peak-to-peak distance of 12.5 nm

Figure 4. The hcp atoms per unit effective contact area as a function of time for at 1st and last contacts with peak-to-peak distance of 12.5 nm. (a) commensurate (001), (b) incommensurate of (001), and (c) (111) surfaces

Figure 5. Tensile strength of metallic bridge as a function length for all surfaces; Open and full symbols represent 1st cycle with fresh asperities and multiple cycle results, respectively. Error bars denote to the standard deviation for multiple contacts.

Figure 6. Defects available before and produced during contact opening as a function of contact length for: a) (001) and b) (111) surfaces. Circles and triangles denote the number of hcp atoms per unit contact area available before opening and their production during opening, respectively. Open symbols

represent the 1st cycle with fresh asperities and full ones show multiple-cycle results. Solid lines represent linear fits of the production of dislocations with contact length L_c and the dashed lines are guided to the eye.

Figure 7. Color online: Snapshots of the first contact cycle for commensurate (001) contacts with different sizes and at various times. The strongest contact size is shown in the middle column. Yellow (light), red (light dark) and blue (dark) spheres denote surface, fcc and hcp atoms respectively. Top and bottom values indicate cross-sectional areas and contact lengths, respectively.

Figure 8. Color online: Snapshots of the first contact cycle for incommensurate (001) contacts with different sizes and at various times. The strongest contact size is shown in the middle column. Yellow (light), red (light dark) and blue (dark) spheres denote surface, fcc and hcp atoms respectively. Top and bottom values indicate cross-sectional areas and contact lengths, respectively.

Figure 9. Color online: Snapshots of the first contact cycle for commensurate (111) contacts with different sizes and at various times. The strongest contact size is shown in the middle column. Yellow (light), red (light dark) and blue (dark) spheres denote surface, fcc and hcp atoms respectively. Top and bottom values indicate cross-sectional areas and contact lengths, respectively.

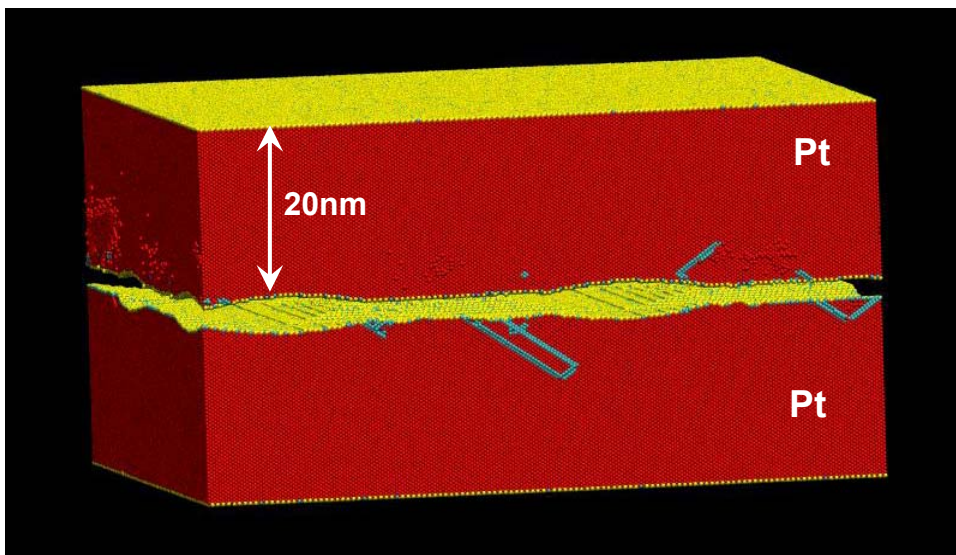


Figure 1

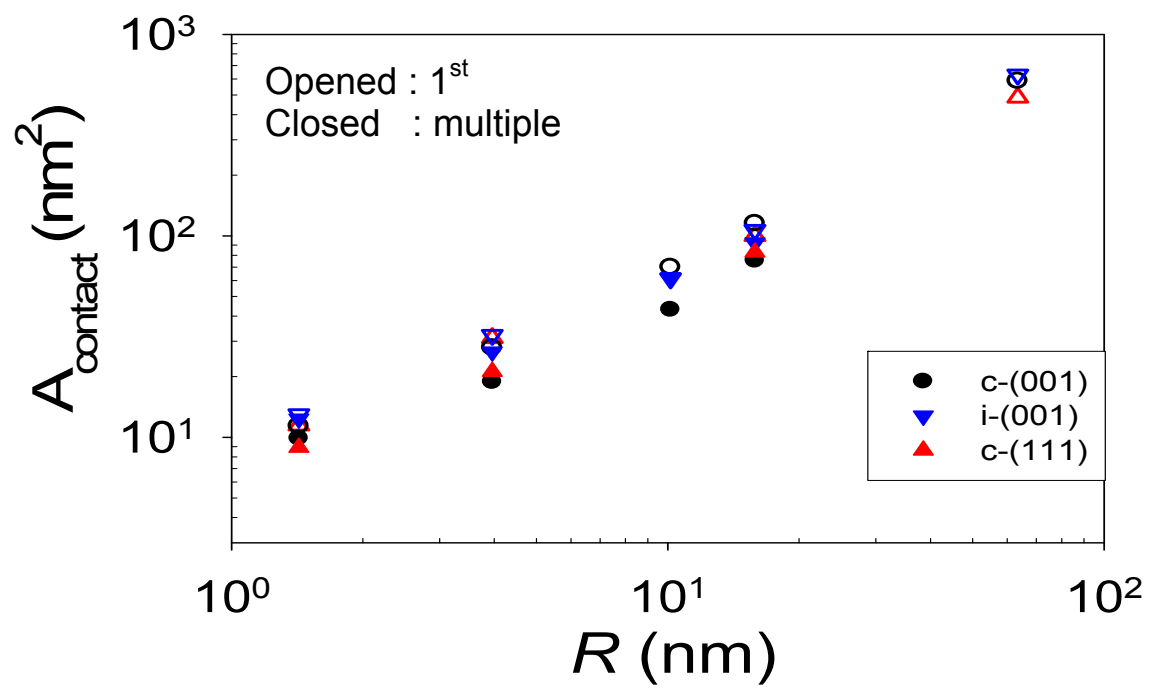


Figure 2

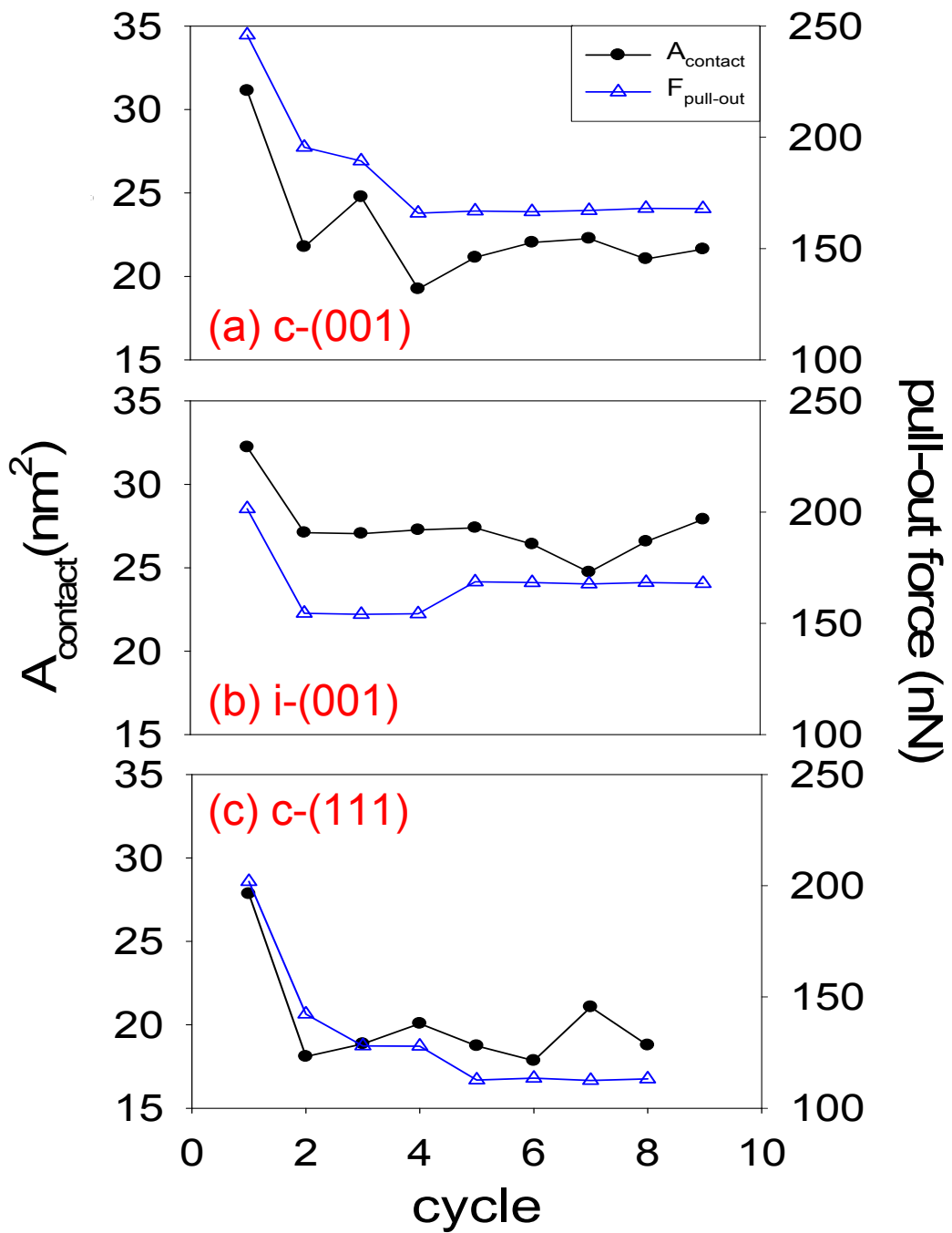


Figure 3.

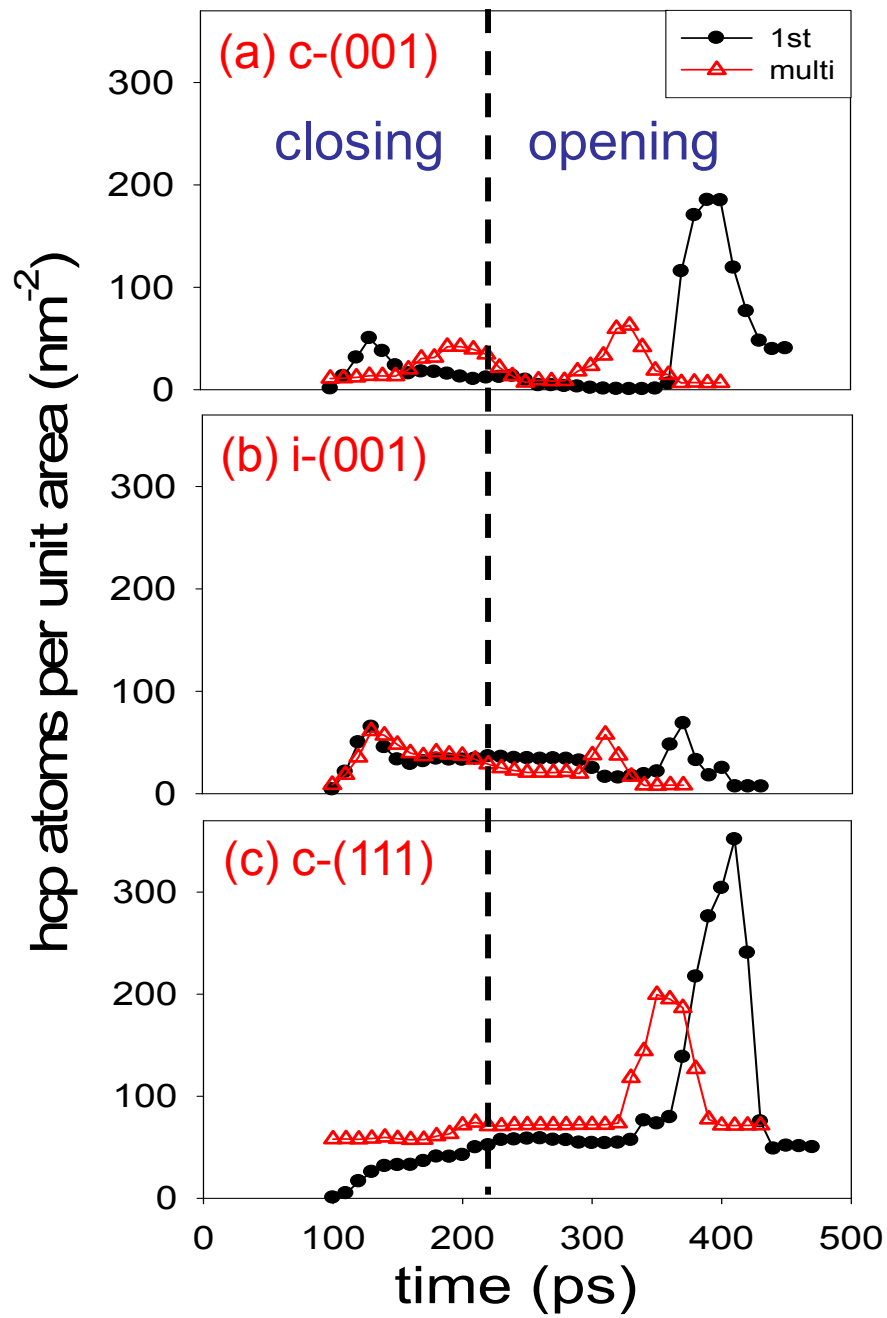


Figure 4

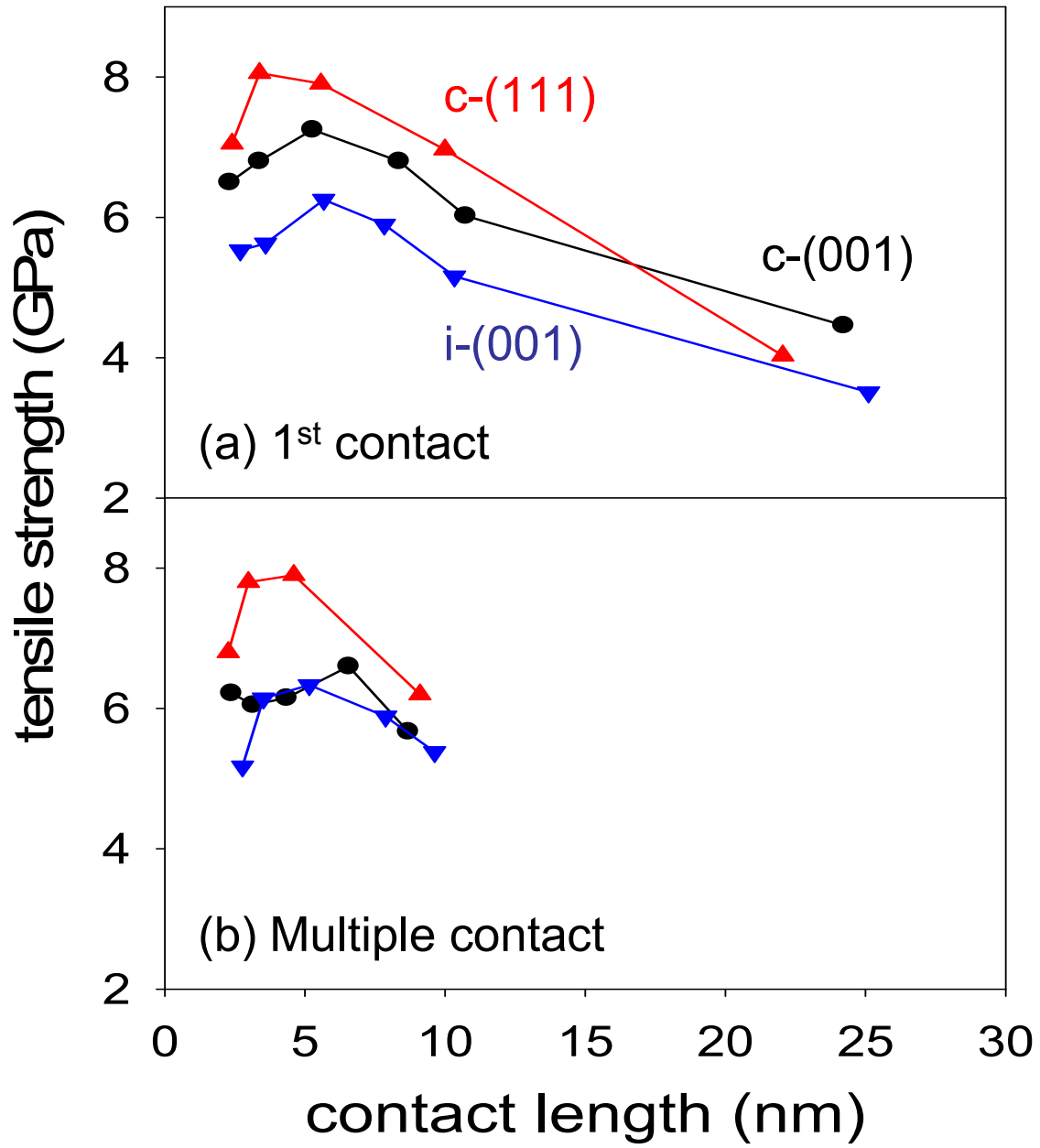


Figure 5

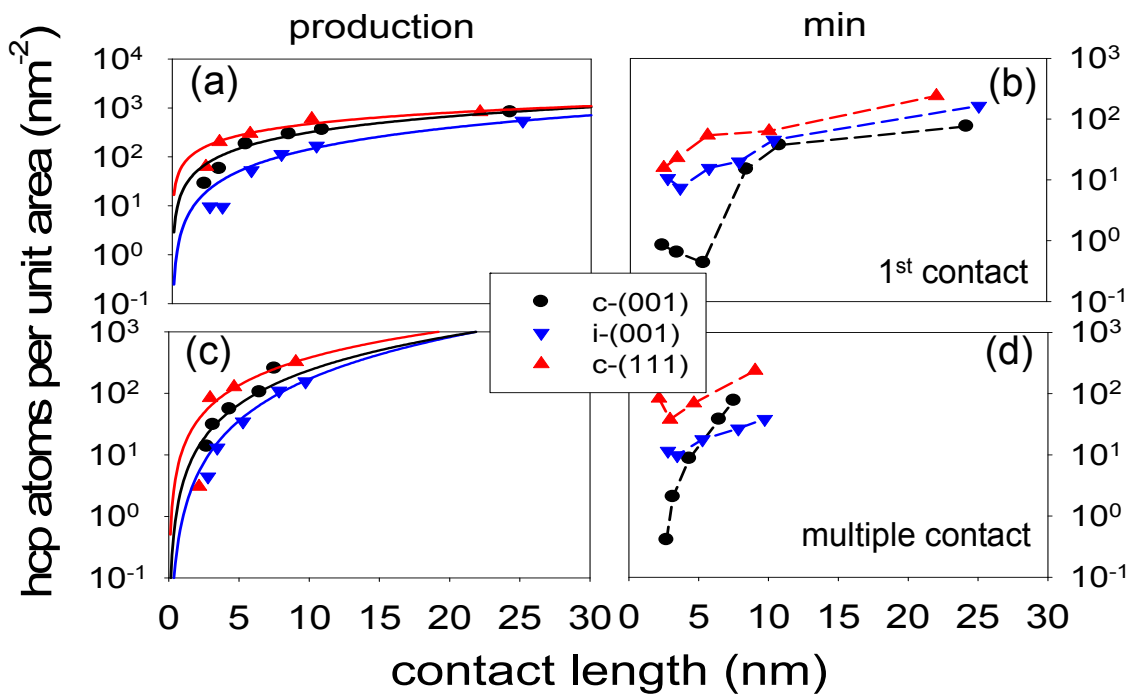


Figure 6

c-(001)

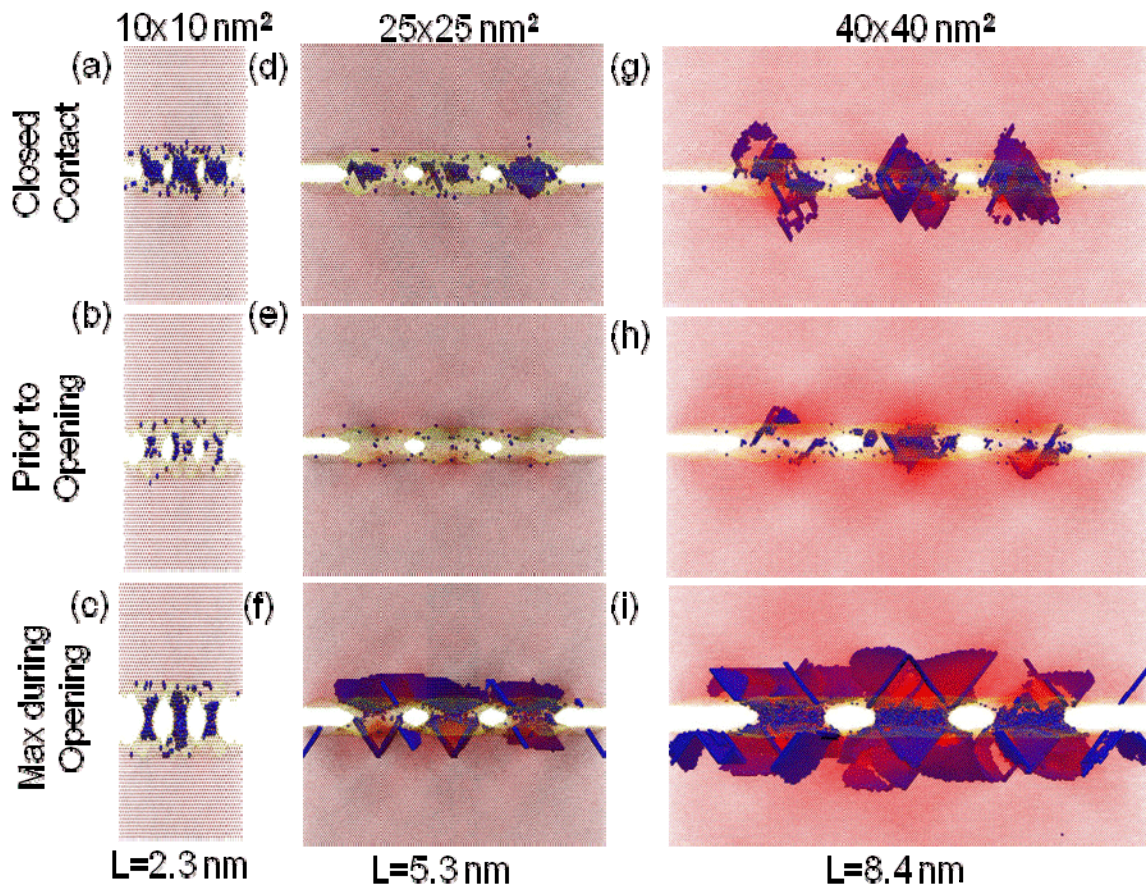


Figure 7

i-(001)

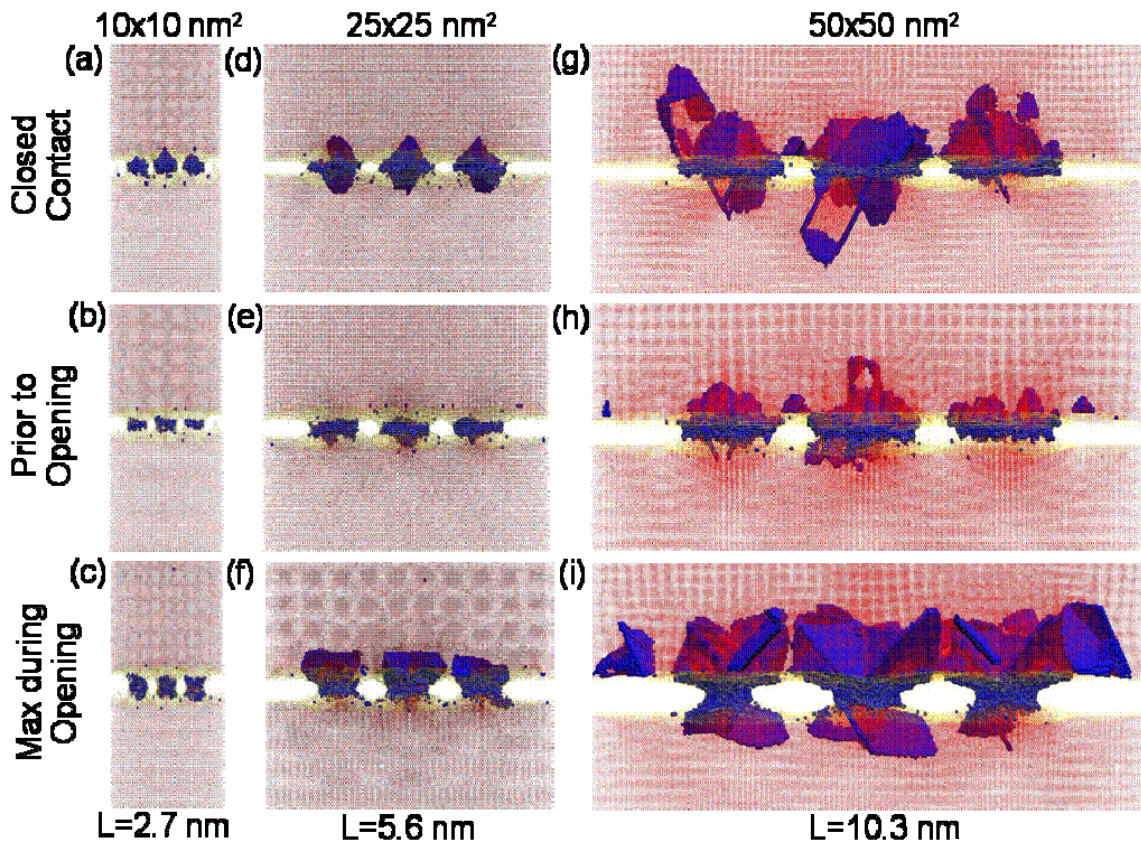


Figure 8

c-(111)

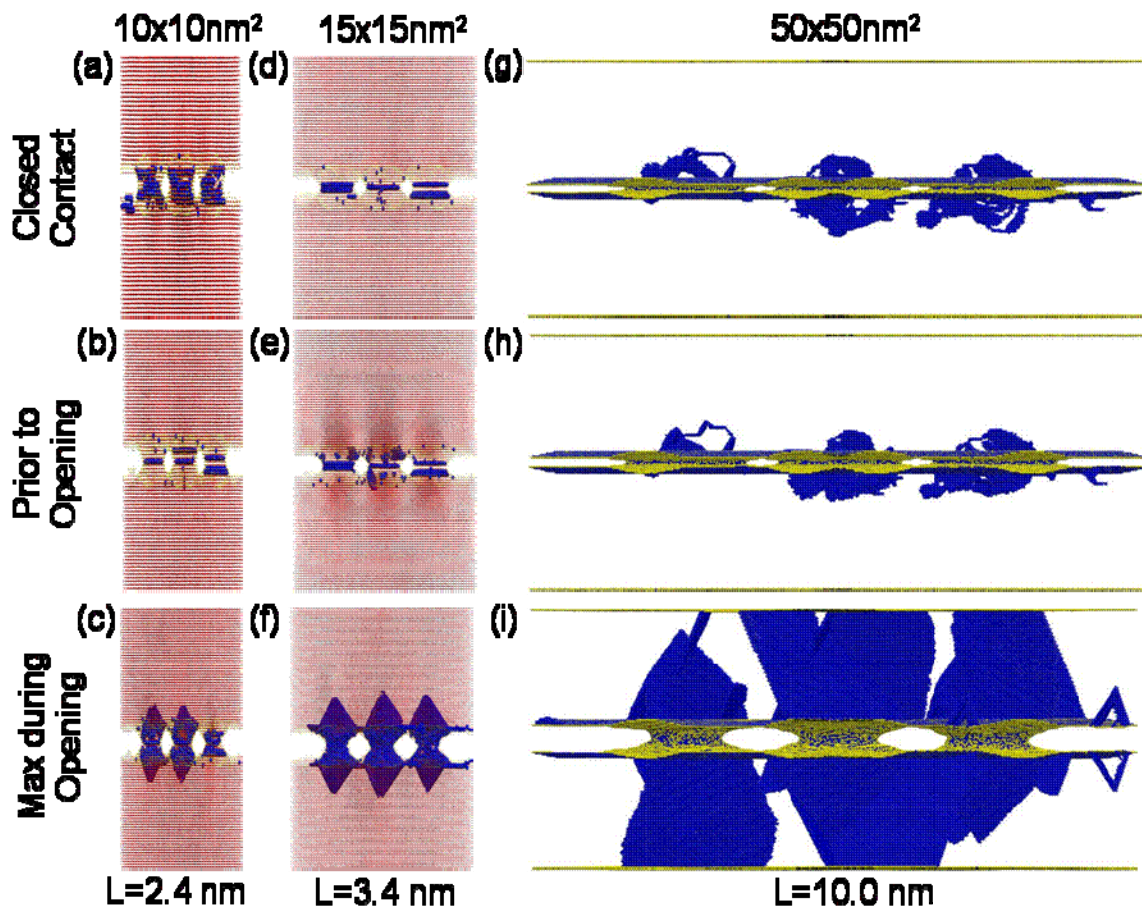


Figure 9

REFERENCES

-
- ¹ C. L. Goldsmith, Z. Yao, S. Eshelman, D. Denniston, IEEE Microwave and Guided Wave Lett. **8**, 269 (1998).
- ² G. M. Rebeiz and J. B. Muldavin, IEEE Microw. Mag. **2**, 59 (2001).
- ³ H. Kam, D. T. Lee, R. T. Howe, T.-J. King, IEDM Tech. Dig. 463 (2005).
- ⁴ A. Zong, Y. Cao, N. Rahbar, W. Soboyejo, J. Appl. Phys. **100**, 104313 (2006).
- ⁵ B. Bhushan, J. Vac. Sci. Technol. B **21**, 2262 (2003).
- ⁶ H. Kim and A. Strachan Phys. Rev. Lett. **104**, 215504 (2010).
- ⁷ P.-R. Cha, D. J. Srolovitz, T. K. Vanderlick, Acta Mater. **52**, 3983 (2004).
- ⁸ J. Song, D. J. Srolovitz, Acta Mater. **55**, 4759 (2007).
- ⁹ G. Binning, H. Rohrer, Ch. Gerber, E. Weibel, Phys. Rev. Lett. **49**, 57 (1982).
- ¹⁰ C. J. Muller, J. M. van Ruitenbeek, L. J. de Jongh, Phys. Rev. Lett. **69**, 140 (1992).
- ¹¹ V. N. Samoilov, I. M. Sivebaek, B. N. J. Persson, J. Chem. Phys. **121**, 9639 (2004).
- ¹² D. Hyman and M. Mehregany, IEEE Transactions on Components and Packaging Technologies **22**, 357 (1999).
- ¹³ S. T. Patton and J. S. Zabinski, Tribol. Lett. **18**, 215 (2005).

-
- ¹⁴ S. J. Plimpton, *J. Comput. Phys.* **117**, 1 (1995).; <http://lammmps.sandia.gov>
- ¹⁵ S. M. Folies, M. I. Baskes, M. S. Daw, *Phys. Rev. B* **33**, 7983 (1986).
- ¹⁶ C. Kelchner, S. J. Plimpton, J. C. Hamilton, *Phys. Rev. B* **58**, 11085 (1998).
- ¹⁷ S. Yip, *Nature Mater.* **3**, 11 (2004).
- ¹⁸ M. S. Allen, J. E. Massad, R. V. Field Jr, and C. W. Dyck, *J. Vib. Acoust.* **130**, 021009, (2008).
- ¹⁹ Y.-Z. Hu, T. Zhang, T.-b. Ma, H. Wang, *Comp. Mater. Sci.* **38**, 98 (2006).
- ²⁰ H. Wang, Y.-Z. Hu, T. Zhang, *Tribol. Int.* **40**, 680 (2007).
- ²¹ J. R. Greer, W. D. Nix, *Phys. Rev. B* **73**, 245410 (2006).
- ²² Z. W. Shan, R. K. Mishra, S. A. Syed Asif, O. L. Warren, A. M. Minor, *Nature Mater.* **7**, 115 (2008).
- ²³ Supplementary material can be found in ...
- ²⁴ G. Gregon and D. R. Clarke, *J. Appl. Phys.* **100**, 094904 (2006).
- ²⁵ S. V. Bobylev and I. A. Ovid'ko, *Phys. Rev. Lett.* **103**, 135501 (2009).